Electronic Supplementary Information

Fabrication of Oxygen-Vacancy Abundant NiAl-Layered Double Hydroxides for Ultrahigh Capacity Supercapacitors

Ziyu Wang[1], Yifan Song[2], Ruiqi Li[1], Risheng Li[2], Runping Jia[2], Kunliang Nie[3], Haijiao Xie[4], Xiaowei Xu[2]*, Lin Lin[1]**

[1]School of Chemical and Environmental Engineering, Shanghai Institute of Technology, Shanghai, 201418, PR China, linlin@sit.edu.cn;

[2]School of Materials Science and Engineering, Shanghai Institute of Technology, Shanghai, 201418, PR China, xiaoweixu@sit.edu.cn;

[3]Sichuan Huachuan Industries Co., Ltd., Chengdu, 610106, PR China, niekunliangep@163.com;

[4]Hangzhou Yanqu Information Technology Co. Ltd., Hangzhou, 310003, PR China

Model and methods of DFT calculation:

We have employed the first-principles[1, 2] to perform all density functional theory (DFT) calculations within the generalized gradient approximation (GGA) using the Perdew-Burke-Ernzerhof (PBE)[3] formulation. We have chosen the projected augmented wave (PAW) potentials[4, 5] to describe the ionic cores and take valence electrons into account using a plane wave basis set with a kinetic energy cutoff of 450 eV. Partial occupancies of the Kohn−Sham orbitals were allowed using the Gaussian smearing method and a width of 0.05 eV. For the optimization of both geometry and lattice size, the Brillouin zone integration was performed with a 0.04 $Å^{-1}$ *k*-mesh Monkhorst-Pack sampling[6]. The self-consistent calculations applied a convergence energy threshold of 10^{-5} eV. The equilibrium geometries and lattice constants were optimized with maximum stress on each atom within 0.02 eV $Å^{-1}$. The 15 Å vacuum layer was normally added to the surface to eliminate the artificial interactions between periodic images. The weak interaction was described by DFT+D3 method using empirical correction in Grimme's scheme[7, 8]. Spin polarization method was adopted to describe the magnetic system. The adsorption energy of adsorbent was calculated as: E_{ads} = E(*adsorbent) - E(*) - E(adsorbent). E(*adsorbent), E(*) and E(adsorbent) represent the total energy of * adsorbent, * and adsorbent molecule, respectively. What's more, the input files and output data of band structure and DOS were generated by the tool——Vaspkit[9].

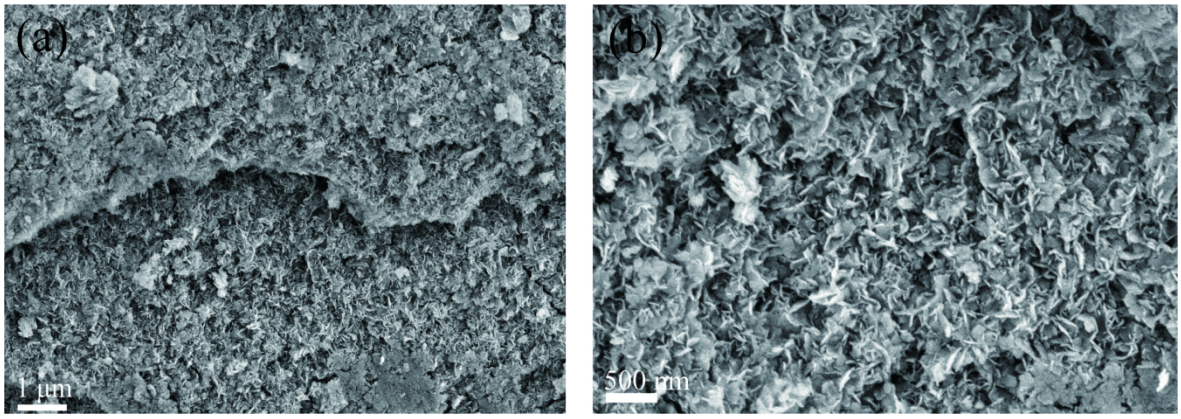

Figure S1. SEM images of NiAl-LDH.

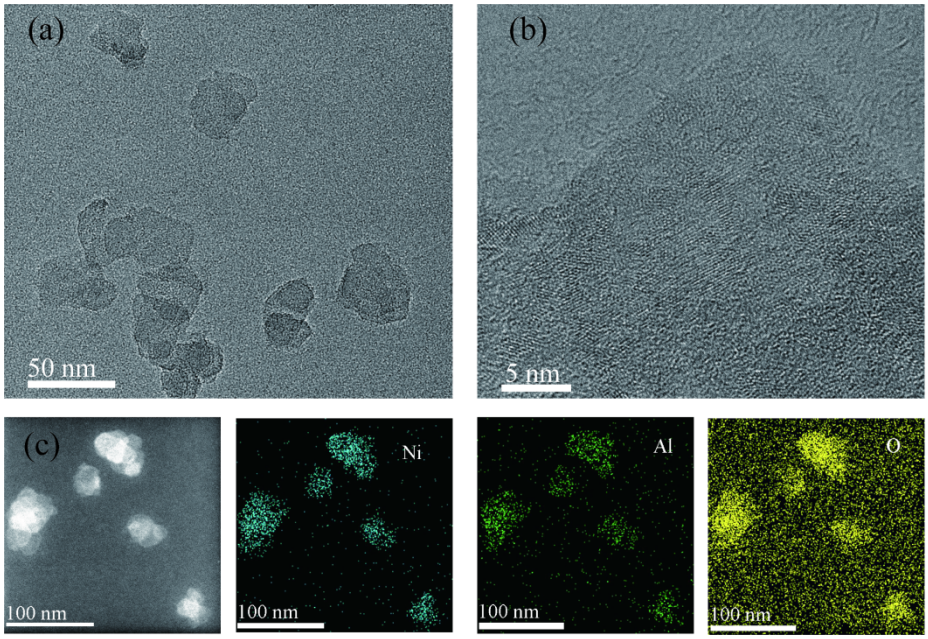

Figure S2. TEM images and EDS mappings of NiAl-LDH.

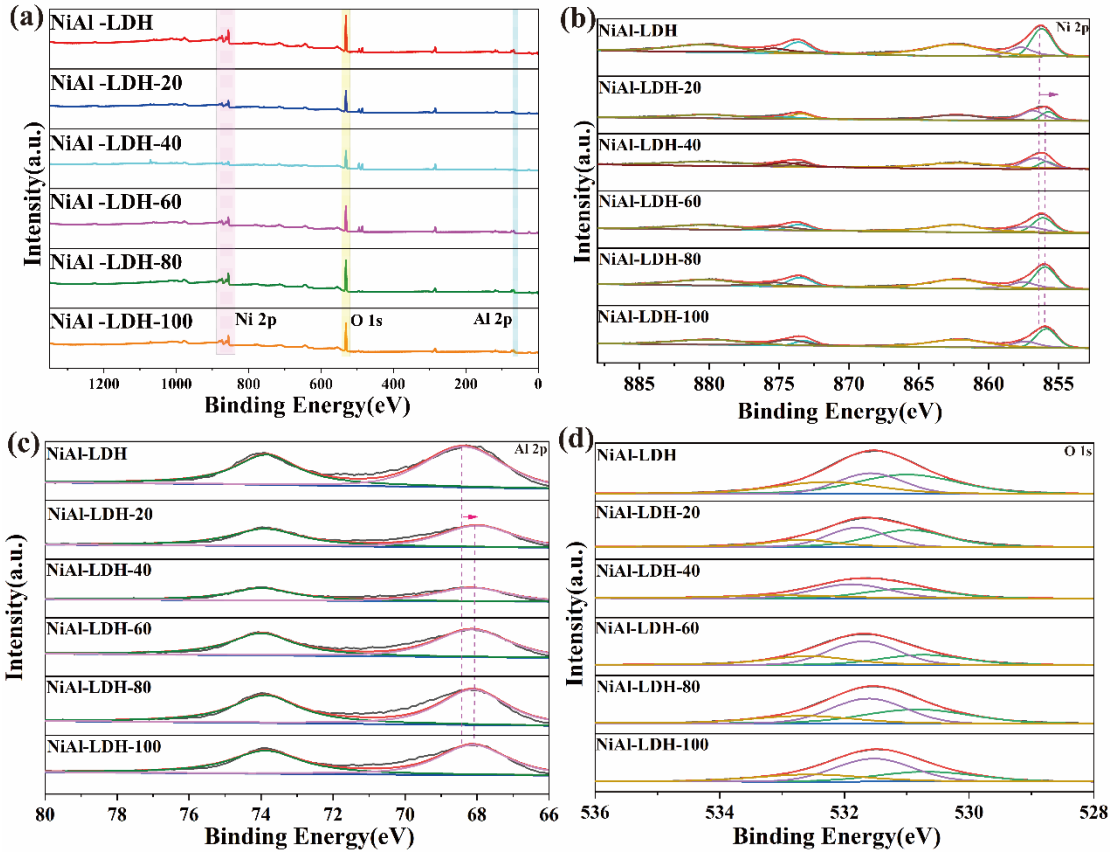

Figure S3. XPS spectra of NiAl-LDH and NiAl-LDH with different vacancy contents: (a) survey spectra, (b) Ni 2p, (c) Al 2p, and (d) O 1s.

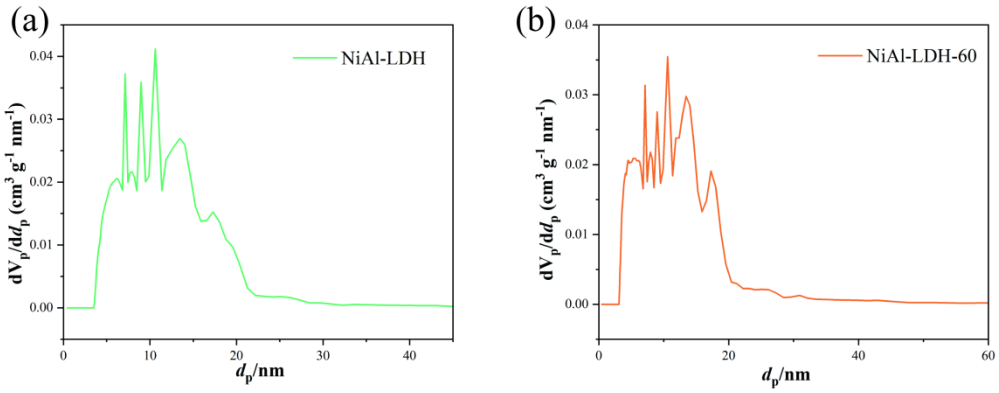

Figure S4. Pore size distribution of (a) NiAl-LDH-60 and (b) NiAl-LDH.

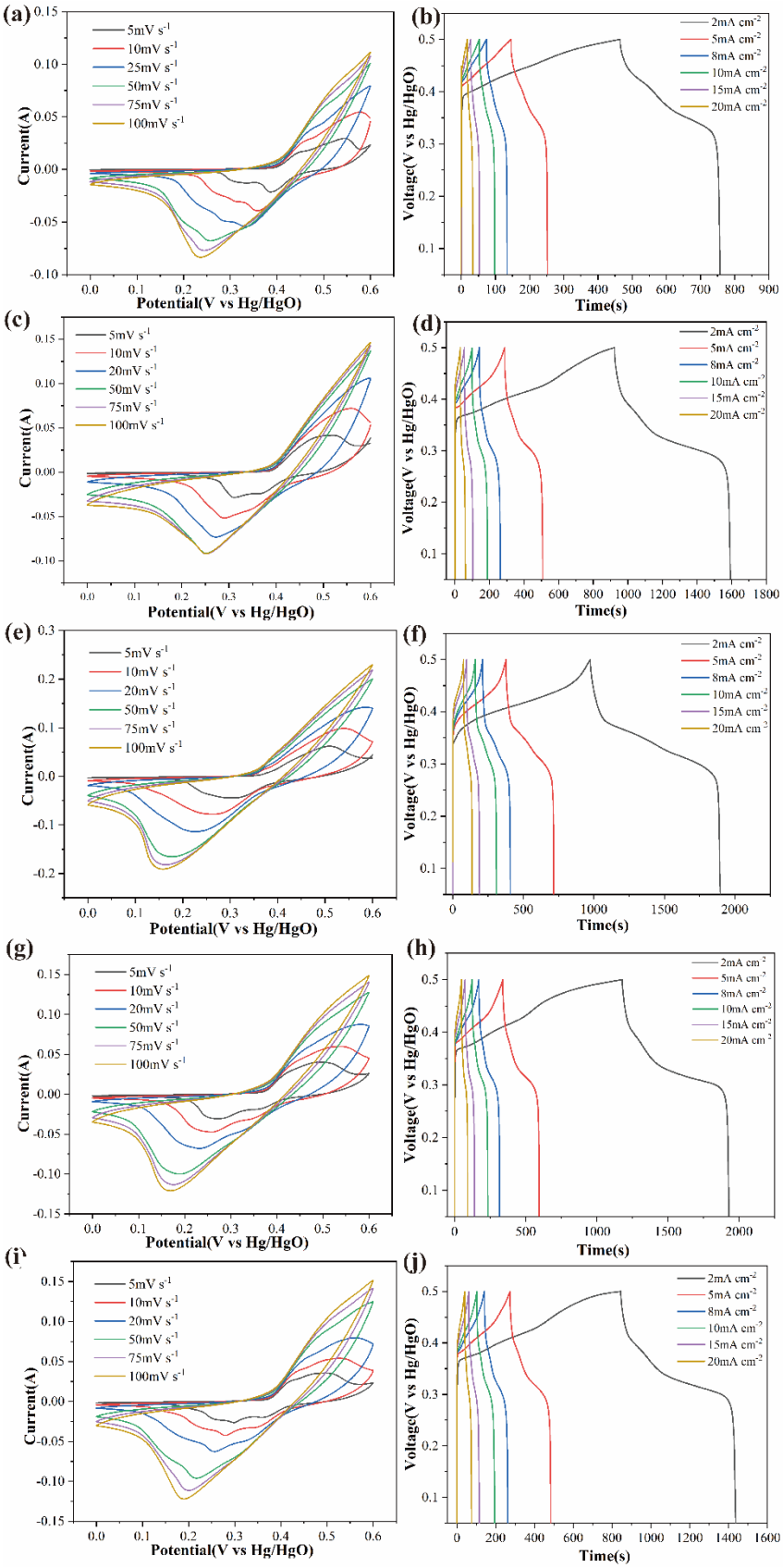

Figure S5. (a) CV and (b) GCD curves of NiAl-LDH; (c) CV and (d) GCD curves of NiAl-LDH-20; (e) CV and (f) GCD curves of NiAl-LDH-40; (g) CV and (h) GCD curves of NiAl-LDH-80; (i) CV and (j) GCD curves of NiAl-LDH-100.

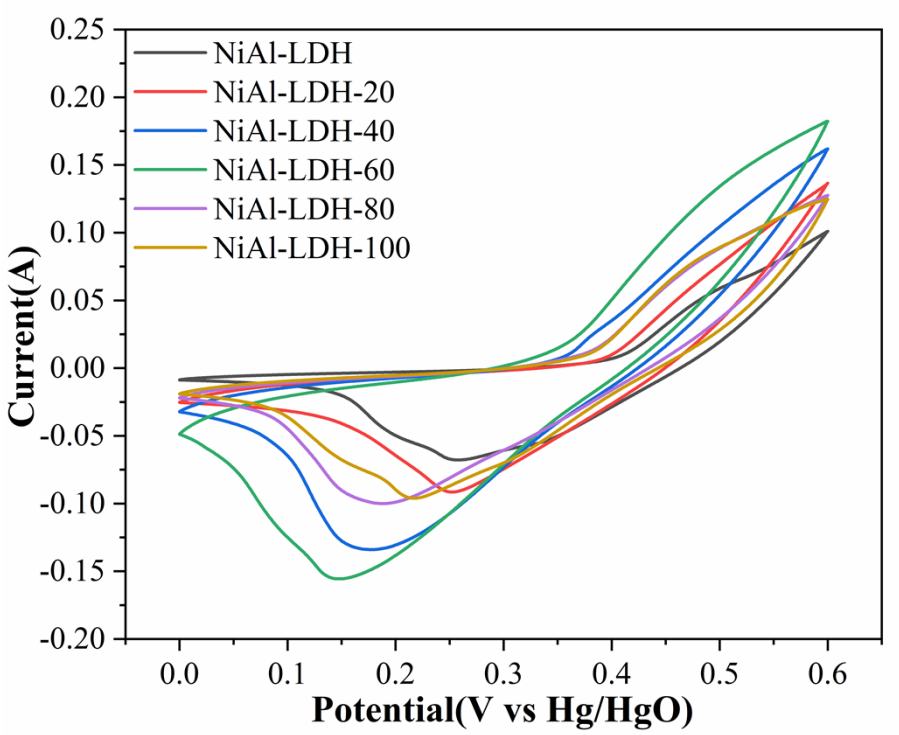

Figure S6. CV comparison plots of NiAl-LDH with different oxygen vacancy concentrations at 50 mV s^{-1} sweep rates.

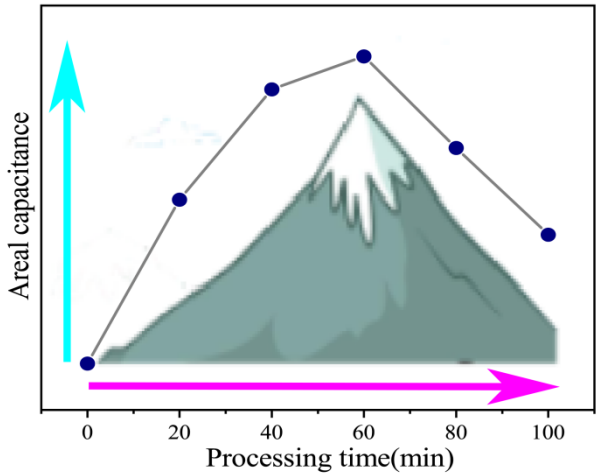

Figure S7. Volcano-type trend of the areal capacitances.

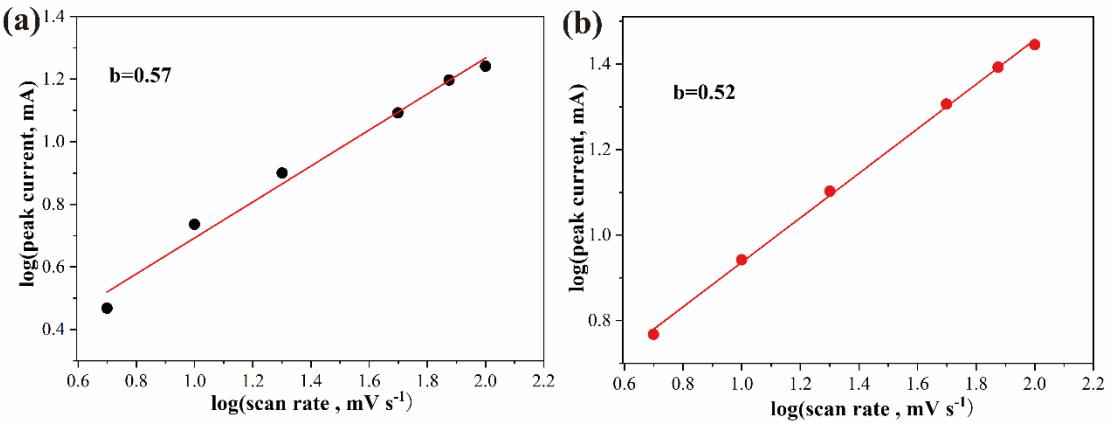

Figure S8. Plot of the anodic peak current density against the scan rate for electrode (a) NiAl-LDH; (b) NiAl-LDH-60.

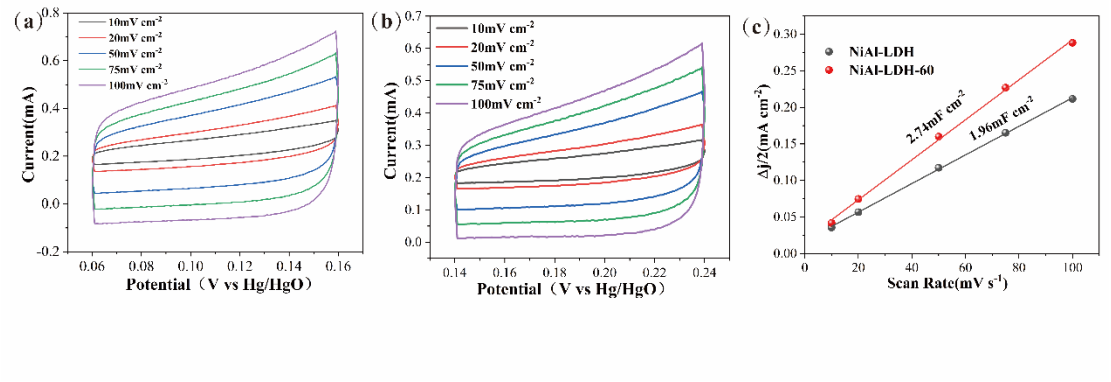

Figure S9. CV curves in the non-faradaic capacitance current range. (a)NiAl-LDH; (b)NiAl-LDH-60; (c) Cdl curves of NiAl-LDH and NiAl-LDH-60.

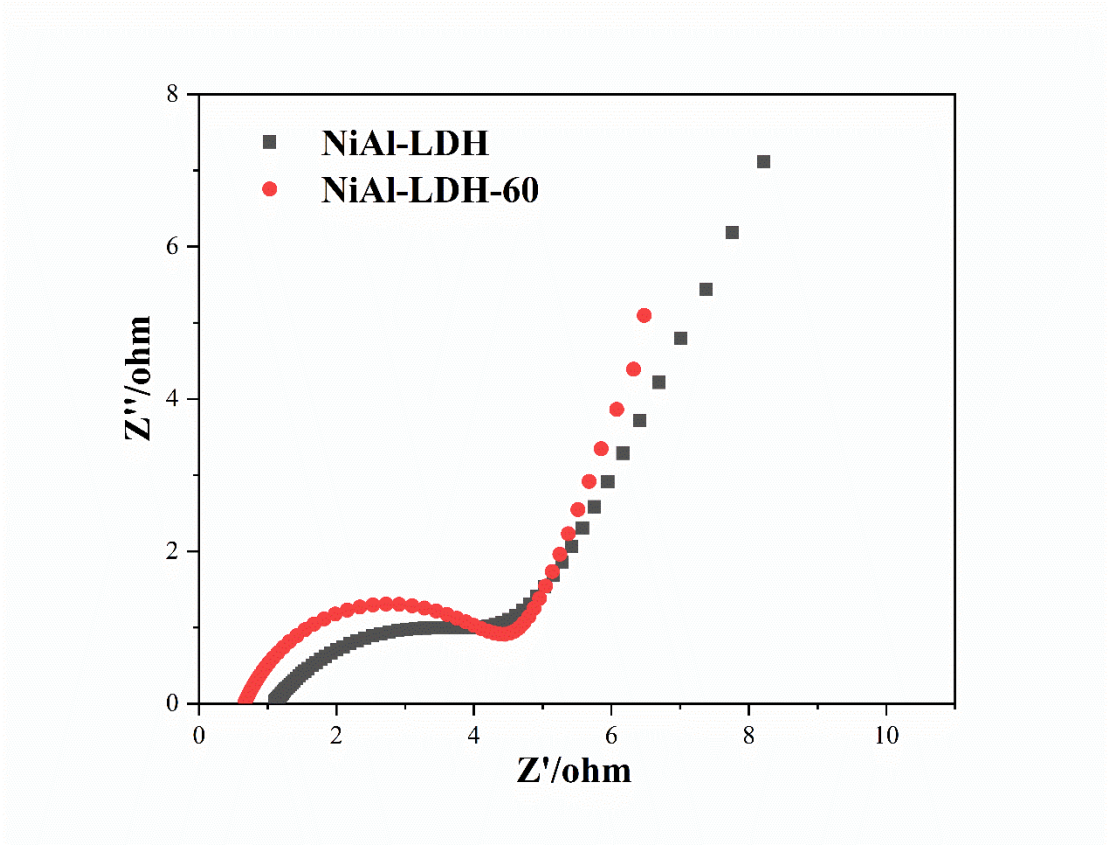

Figure S10. EIS plots for NiAl-LDH and NiAl-LDH-60.

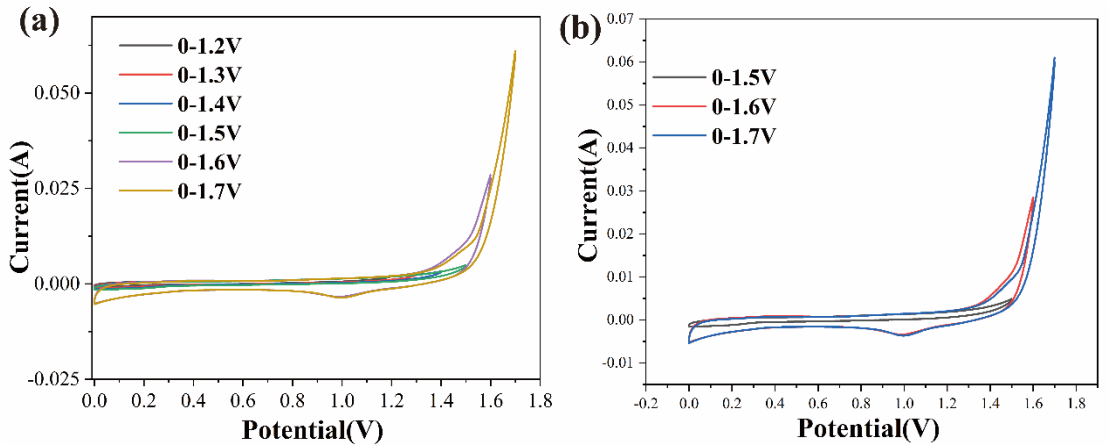

Figure S11. (a) CV curves at a scan rate of 100 mVs $^{-1}$underdifferent voltage windows (0-1.2 V to 0-1.7 V; (b) voltage windows of 1.5V, 1.6V and 1.7V.

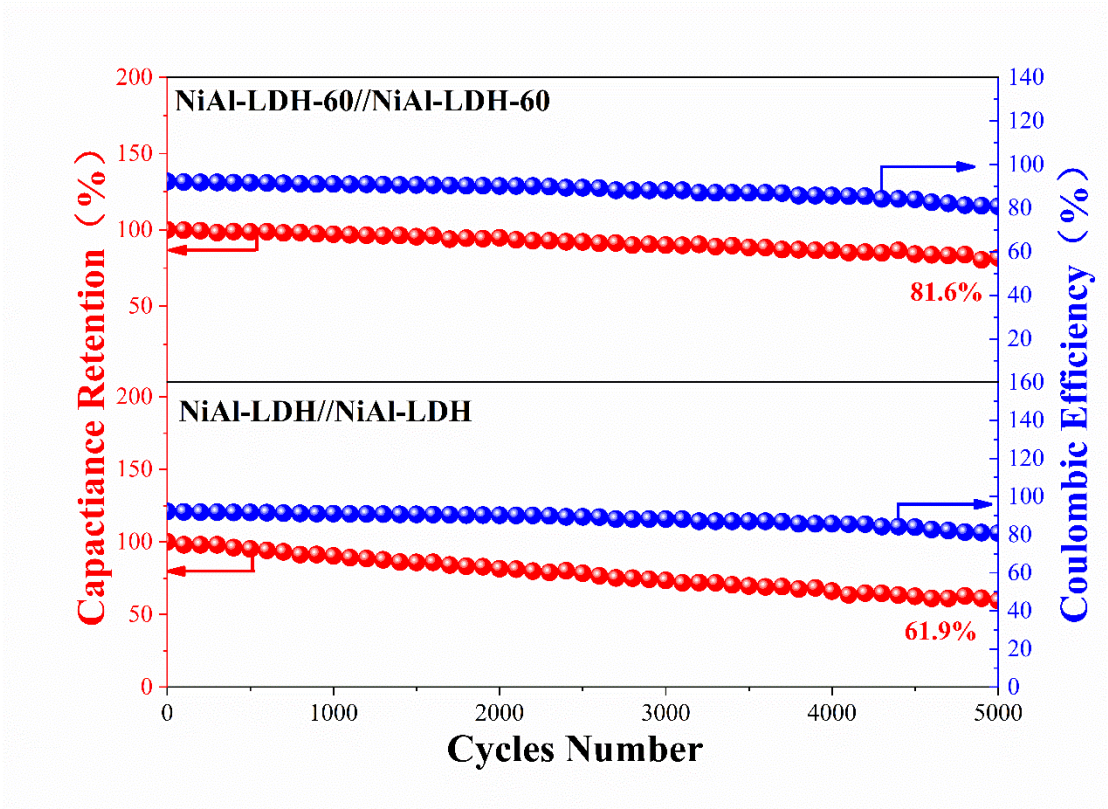

Figure S12. Cycling performance of the SSC device.

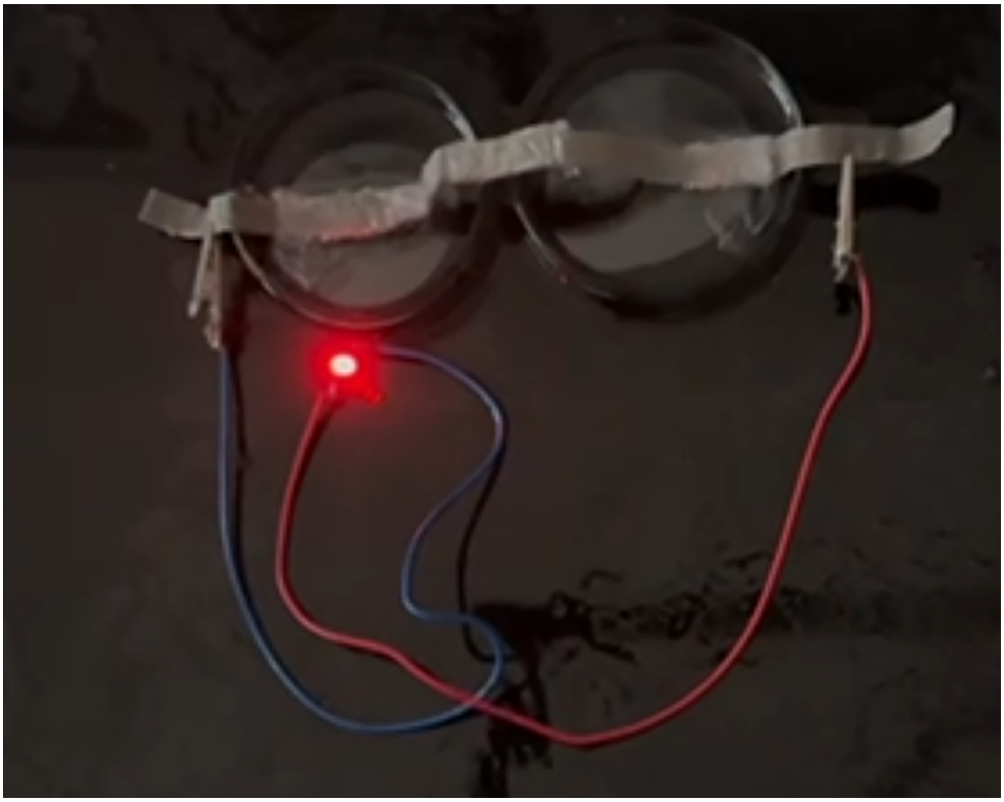

Figure S13. Real application of two as-prepared SSC devices in series to light up a red LED indicator.

Table S1. Adsorption energy of NiAl-LDH-60

Units (eV)	The first OH-	The second OH-
E(OH)	-7.7290	-7.7290
E(slab)	-659.4136	-671.1244
E(slab*OH)	-671.1244	-683.1926
E(ads)	-3.9817	-4.3392

References:

[1] Kresse, G.; Furthmuller, J., Efficient iterative schemes for ab initio total-energy calculations using a plane-wave basis set. *Phys Rev B Condens Matter* **1996,** *54* (16), 11169-11186.

[2] Kresse, G.; Furthmüller, J., Efficiency of ab-initio total energy calculations for metals and semiconductors using a plane-wave basis set. *Computational Materials Science* **1996,** *6* (1), 15-50.

[3] Perdew, J. P.; Burke, K.; Ernzerhof, M., Generalized Gradient Approximation Made Simple. *Phys Rev Lett* **1996,** *77* (18), 3865-3868.

[4] Kresse, G.; Joubert, D., From ultrasoft pseudopotentials to the projector augmented-wave method. *Physical Review B* **1999,** *59* (3), 1758-1775.

[5] Blochl, P. E., Projector augmented-wave method. *Phys Rev B Condens Matter* **1994,** *50* (24), 17953-17979.

[6] Monkhorst, H. J.; Pack, J. D., Special points for Brillouin-zone integrations. *Physical Review B* **1976,** *13* (12), 5188-5192.

[7] Grimme, S.; Antony, J.; Ehrlich, S.; Krieg, H., A consistent and accurate ab initio parametrization of density functional dispersion correction (DFT-D) for the 94 elements H-Pu. *J Chem Phys* **2010,** *132* (15), 154104.

[8] Grimme, S.; Ehrlich, S.; Goerigk, L., Effect of the damping function in dispersion corrected density functional theory. *J Comput Chem* **2011,** *32* (7), 1456-65.

[9] Wang, V.; Xu, N.; Liu, J.-C.; Tang, G.; Geng, W.-T., VASPKIT: A user-friendly interface facilitating high-throughput computing and analysis using VASP code. *Computer Physics Communications* **2021,** *267*.